

# Journal of Materials Chemistry A

Accepted Manuscript



This is an *Accepted Manuscript*, which has been through the Royal Society of Chemistry peer review process and has been accepted for publication.

*Accepted Manuscripts* are published online shortly after acceptance, before technical editing, formatting and proof reading. Using this free service, authors can make their results available to the community, in citable form, before we publish the edited article. We will replace this *Accepted Manuscript* with the edited and formatted *Advance Article* as soon as it is available.

You can find more information about *Accepted Manuscripts* in the [Information for Authors](#).

Please note that technical editing may introduce minor changes to the text and/or graphics, which may alter content. The journal's standard [Terms & Conditions](#) and the [Ethical guidelines](#) still apply. In no event shall the Royal Society of Chemistry be held responsible for any errors or omissions in this *Accepted Manuscript* or any consequences arising from the use of any information it contains.

# Soft-template synthesis of 3D porous graphene foams with tunable architectures for lithium-O<sub>2</sub> battery and oil adsorption applications

Cite this: DOI: 10.1039/x0xx00000x

Received 00th February 2014,  
Accepted 00th February 2014

DOI: 10.1039/x0xx00000x

www.rsc.org/

Xiaodan Huang<sup>a,b</sup>, Bing Sun<sup>a</sup>, Dawei Su<sup>a</sup>, Dongyuan Zhao<sup>\*b</sup> and Guoxiu Wang<sup>\*a</sup>,

We report a general emulsion soft-template method to synthesize porous graphene foams for multi-functional applications, including lithium-oxygen battery and oil-adsorption. Multiple micro-emulsions and micelles were employed to produce three-dimensional porous graphenes with well-tailored inter architectures for the first time. Detailed mechanism study reveals that specific interfacial interactions, such as  $\pi$ - $\pi$  interaction, hydrophobic affinity or electrostatic interaction, are vital for the formations of porous graphene materials. When applied as cathode materials in lithium-oxygen batteries, the porous graphene foams exhibited a good catalytic activity. Besides, the porous graphene materials also demonstrated the capability for oil adsorption with a high efficiency.

## Introduction

The design and synthesis of three-dimensional (3D) graphene architectures with controlled porous textures have attracted extensive research owing to the combined functionalities of graphene frameworks and highly porous nanostructures.<sup>1-9</sup> Templates play pivotal roles in the pore generating process.<sup>10-13</sup> Based on their physical properties, templates can be generally classified as two groups: rigid nanostructure solids (hard-templates) and supramolecular aggregates, such as emulsions and micelles (soft-templates). Currently, 3D porous graphene materials are mainly prepared by hard-template methods. Porous metal foams (Ni foam assisted chemical vapour deposition<sup>9,14-16</sup>), solid nanostructure particles (silica spheres<sup>17</sup> or polymer particles<sup>18-20</sup>) and coagulated solvents (freeze-drying<sup>2-6,8</sup>) are usually employed as hard-templates to synthesize porous graphenes with different pore sizes and morphologies.

Compared with the hard-template approach, the soft-template method has many advantages, such as easy processing, high efficiency and low-cost.<sup>21,22</sup> More importantly, soft-templating methods are always associated with complex interfacial reactions, which can provide an excellent platform to investigate the principle interfacial chemistries. However, to date, 3D porous graphene materials prepared through the soft-template route is rarely reported. The “breath-figure” method, referring to the use of condensed aqueous droplets as templates to fabricate honeycomb-like macroporous graphene,<sup>7,23</sup> is quite

close to the concept of soft-template. Yet, the pore size control capability is poor and the commonality of this method is still limited. The difficulties of preparing porous graphene by the soft-template route can be ascribed to the inherent properties of graphene. Unlike conventional porous silicas or carbons, the precursors of graphene materials, such as graphene oxide nanosheets, are usually bulk instead of molecular precursors or polymer oligomers. When assembling with templates, the bulk structural feature of graphene precursors could cause difficulties for the regular assembly. Therefore, specific affinities are required to enhance the interactions between graphene precursors and soft-templates in order to achieve successful assemblies.

Herein, we demonstrate, for the first time, a general emulsion soft-template approach to synthesize 3D porous graphene foams (PGFs) with tunable pore structures. Multiple micro-emulsions and micelles with rationally designed surface properties are employed as soft-templates to generate porosity in graphene frameworks. Diverse templates render PGFs with adjustable pore diameters (from several micrometers to tens of nanometers), high surface area and large pore volume. Besides the novel structural features, PGFs also exhibit promising performances for oil adsorption and lithium-oxygen (Li-O<sub>2</sub>) battery applications.

## Experimental

### Materials syntheses

**Synthesis of PGF-1:** In a typical synthesis process, TMB (6.0 ml) was added to HCl solution (2.0 M, 100 ml) and stirred continuously for 30 min at 25 °C. Then, the mixture was sonicated for 30 min to form a cloudy suspension. Graphene oxide solution (60 ml, 5.0 mg ml<sup>-1</sup>) and distilled H<sub>2</sub>O (40 mL) were mixed with the TMB emulsion suspension at room temperature. After, the precipitate was collected by vacuum filtration. The obtained precipitate was firstly sintered at 350 °C in argon for 5 h and further heated at 900 °C for another 5 h under argon atmosphere to obtain the final product, PGF-1.

**Synthesis of PGF-2:** Typically, n-hexadecane (4.88 ml) was added to HCl solution (2.0 M, 300 ml) and stirred continuously for 30 min at 25 °C. Then, the mixture was sonicated for 30 min to form a cloudy suspension. Graphene oxide solution (90 ml, 5.0 mg ml<sup>-1</sup>) and distilled H<sub>2</sub>O (10 mL) were mixed with the n-hexadecane emulsion suspension at room temperature. After, the precipitate was collected by vacuum filtration. The obtained precipitate was firstly calcined at 350 °C in argon for 5 h and further heated at 900 °C for another 5 h under argon atmosphere to obtain the final product, PGF-2.

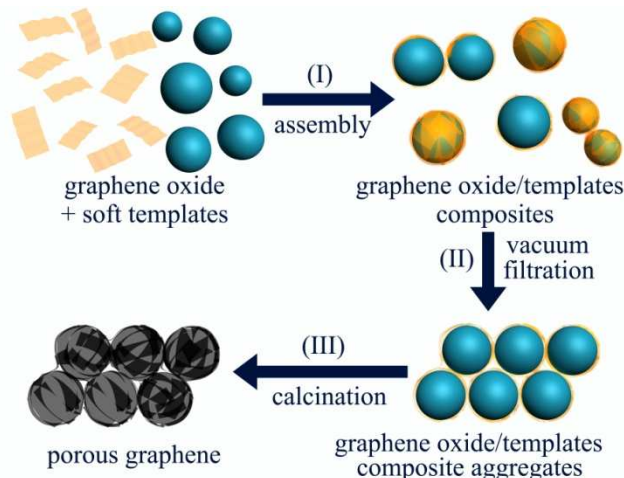
### Materials characterization

Scanning electron microscopy observations were performed on a field emission scanning electron microscopy (FESEM, Zeiss Supra 55VP). Transmission electron microscopy characterisation was conducted using a JEM-2100 transmission electron microscope operated at 200 kV. Optical microscopy images were recorded by an Olympus BX51 microscope under bright field and a WB-#2 filter cube. The N<sub>2</sub>-sorption measurement was carried out at 77 K with a Micromeritics 3Flex Surface Characterization Analyser. The zeta-potentials were measured at 25 °C by a Nanosizer ZS-90 instrument (Malvern). X-ray diffraction (XRD) patterns were recorded on a Siemens D5000 X-ray diffractometer with Ni-filtered Cu K $\alpha$  radiation ( $\lambda=1.54056$  Å). The electrical conductivity was tested by a four-point probe method with a model 2000 6½-digit Keithley Multimeter.

### Electrochemical testing

The catalyst cathodes were prepared as follows: PGFs powder (90 wt%) was mixed with poly(tetrafluoroethylene) (PTFE) (10 wt%) in isopropanol to form a slurry. The slurry was then coated onto a glass fibre separator. The cathode film was punched into discs with a diameter of 14 mm and dried at 110 °C in a vacuum oven. A Swagelok cell with an air hole (0.785 cm<sup>2</sup>) on the cathode end was used to assemble Li-O<sub>2</sub> batteries. The cells were assembled in an Ar-filled glove box. A lithium foil was used as the anode. Glass filters soaked with LiClO<sub>4</sub> the (0.1 M) Dimethyl sulfoxide (DMSO) solution were used as separators. Measurements were conducted in dry oxygen atmosphere (1 atm). Galvanostatic discharge-charge tests were carried out on a Neware battery testing system. The specific capacity was calculated based on the mass of PGFs.

### Results and discussion



**Scheme 1.** Schematic illustration of the emulsion soft-template synthesis procedures for preparing porous graphene foams (PGFs). (I) Self-assembly occurs between graphene oxide and emulsion soft-templates; (II) Separation of graphene oxide/template composites. (III) Calcination to produce PGFs.

The emulsion soft-template method is schematically illustrated in Scheme 1. Due to the ease of processing and the rich surface functional groups, graphene oxide (GO) was used as the precursor of graphene. Well-chosen emulsions and micelles were adopted as soft-templates to fabricate graphene foams. By simply mixing GO and templates in aqueous solutions, rationally designed affinities initiated the self-assembly (GO sheets wrapping on templates) spontaneously. The composites obtained in the assembly step were separated from suspensions by vacuum filtration and subsequent calcination under inert atmosphere, resulting in the porous foams constructed by reduced graphene oxide sheets. The final products are denoted as PGF-x, with x being different samples with controlled pore structures.

A typical product PGF-1 was prepared by using 1, 3, 5-Trimethylbenzene (TMB) micro-emulsions as the soft-templates. TMB emulsions were generated by ultra-sonication treatment in 2M HCl aqueous solution (Fig. S1), which have a spherical morphology with diameters of several micrometres (Fig. S2A). Flat GO sheets with an average height of ~ 1.2 nm (Fig. S3) were employed as the precursor for porous graphene foams. The  $\pi$ -conjugation and the hydrophobic nature of TMB allow micro-emulsions to react with the poly-aromatic domains in the central plane of GO through both  $\pi$ - $\pi$  interaction and hydrophobic affinity.<sup>17,24,25</sup> Scanning electron microscopy (SEM) images of PGF-1 clearly show a highly porous structure in a large sample area (Fig. 1A, B and Fig. S4). The pores exhibit a polyhedral morphology with sizes of several micrometres, which is well matched with the diameter of TMB emulsions. In Fig. 1B, cavities located at the junctions of pore walls (indicated by arrows) can be clearly identified, suggesting that 3D architectures were constructed by packing graphene nanosheets. The transmission electron microscopy (TEM) image (Fig. 1C) shows an open pore of PGF-1 with wrinkled graphene layers of pore walls. The TEM images of a crashed piece of PGF-1 (Fig. 1D and E) show a junction of three neighbouring pores. The wrinkled graphene sheets were interlaced around the pore to build up the skeleton of PGF-1. Identified by the contrast differences in the magnified TEM picture of the junction (Fig. 1E), the pore walls (indicated by

arrows) are estimated to be  $\sim 10$  nm. The high-resolution transmission electron microscopy (HR-TEM) image of the pore wall (Fig. 1F) exhibits typical fringes of lamellar lattices in multi-layer graphene sheets (marked by the black arrow), recommending that the porous foam was solidified by forming multi-layer graphene walls during the calcination step.

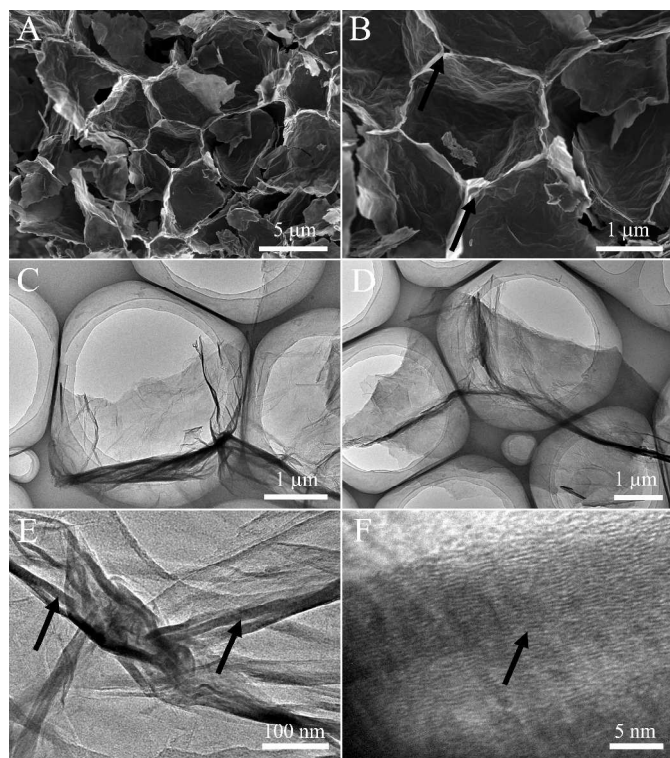


**Figure 1.** Electron microscopy characterizations of PGF-1 synthesized from TMB emulsion template. Typical SEM images in low (A) and high (B) magnifications. TEM images of one macropore (C) and a pore wall joint (D). High magnification TEM image (E) and high resolution TEM image (F) of pore walls in PGF-1.

The in-situ interactions between GO and emulsion templates were observed by an Olympus BX5 microscope (Fig. S2). After mixing the cloudy TMB emulsion suspension with transparent GO aqueous solution, a light-yellow floccule separated out spontaneously and floated on the upper-layer (Fig. S5), indicating a complete self-assembly of GOs and TMB emulsions. Under the observation of optical microscopy in bright field, the floccule suspension shows a very similar view to pristine emulsion suspension (Fig. S2B). When an excitation light (450 — 480 nm) was provided, the image of the same area displayed a completely different picture. Yellow fluorescence emitted from graphene oxides<sup>26,27</sup> can be observed (Fig. S2C). In the combined image (Fig. S2D), it is clearly seen that TMB emulsions, especially several individual ones, are tightly wrapped by thin, yellow GO sheets, suggesting strong specific affinities between GO nanosheets and TMB templates.

Further experiments were conducted to demonstrate the delicate balance among GOs, TMB emulsions and acidic aqueous environments. When TMB emulsions were absent, only lamellar assembled graphene sheets with a mildly wrinkled surface were obtained after the same synthesis procedure, revealing the indispensability of TMB templates

(Fig. S6). While mixing emulsions and GO in a neutral solution, a homogeneous suspension was formed instead of a floatable floccule precipitation (Fig. S7A). The homogeneity of suspension induced a very slow filtration process. Although the product separated at the early filtration process exhibited a good porous structure after calcination, the significantly prolonged filtration time eventually caused the phase separation in the majority of suspensions (Fig. S7). The function of acid is to break the electrostatic balance of GO sheets in solution<sup>28, 29</sup> and enhance the interaction between GO and soft-templates. Salts, such as potassium chloride (KCl), can play a similar role in the PGF-1 preparation (Fig. S8). However, such a high concentration of KCl is difficult to be completely removed and this could cause contamination in final materials. Other acid, such as H<sub>2</sub>SO<sub>4</sub> (2 M) was applied as well, resulting a similar large macroporous architecture (Fig. S9), which further proved the hypothesis of acid function.

By employing different emulsion templates, the pore morphologies and the surface properties can be varied spontaneously. N-hexadecane (HD) is an alkane hydrocarbon with a chain of 16 carbon atoms. The hydrophobic interaction becomes the main driving force in directing the assembly of n-hexadecane emulsions and GO sheets. Through blend, separation and calcination steps, graphene foam with a hierarchical porous structure was obtained, denoted as PGF-2. Ultra-large macropores of  $\sim 100$   $\mu\text{m}$  can be observed in the low-magnification SEM images (Fig. 2A and Fig. S10). The close observation of PGF-2 reveals that this sample is highly porous inside (Fig. 2B). The ultra-large pore skeleton consists of numerous “small” pores, forming a two-level hierarchical porous architecture. As shown in Fig. 2C, the relatively small pores are constructed from thin graphene layers, with a pore size within 5  $\mu\text{m}$ . TEM images of PGF-2 show obvious hierarchical porosity information as well. Inside the pores, frames of small pores with a diameter of  $\sim 1$   $\mu\text{m}$  can be clearly identified (Fig. 2D, E and F). The dramatic structural differences between PGF-1 and PGF-2 samples might be attributed to the natures of two templates. Unlike the extra  $\pi$ - $\pi$  interaction offered by TMB, HD can only react with GO through hydrophobic interaction. This relatively weak affinity would cause HD template partially maintains large size ( $\sim 100$   $\mu\text{m}$ ) droplets as conventional HD emulsions,<sup>30</sup> leading to the generation of ultra-large macropores in PGF-2.

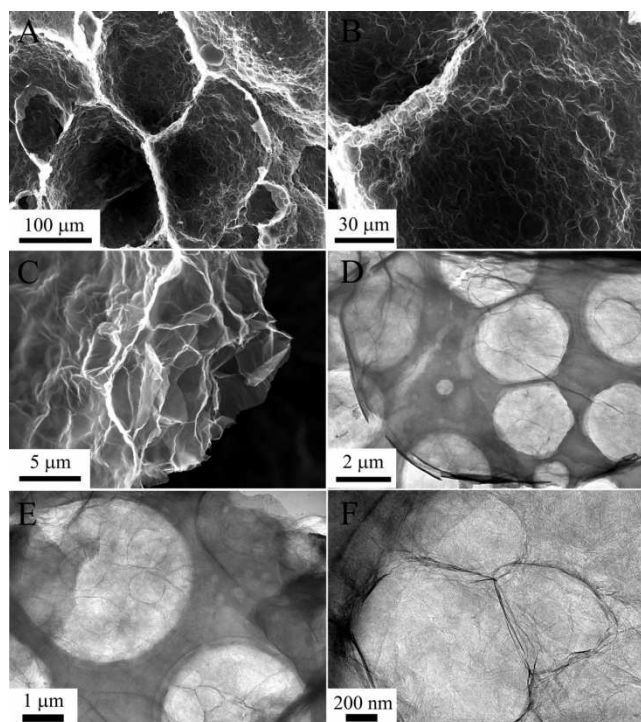


**Figure 2.** Electron microscopy characterizations of PGF-2 synthesized from n-hexadecane emulsion template. (A), (B) and (C) are typical SEM images of PGF-2 with different magnifications, from low to high. (D), (E) and (F) are TEM images of PGF-2 in different resolutions.

When a hydrophobic silane - dimethyldimethoxysilane (DMDMS) - was used to generate the template emulsions, we obtained highly porous graphene foam with uniform distribution of silica nanoparticles on the surface (PGF-3). SEM and elemental mapping analysis confirmed the homogeneous distribution of silica nanoparticles on graphene walls and macroporous graphene foam ( $\sim 4 \mu\text{m}$ , Fig. S11, Fig. S12). The excellent assembling of GO sheets and DMDMS emulsions further supports the soft-template scheme.

To achieve the control of pore size, surfactants were used to adjust the diameters of the emulsion templates. By strong ultrasonic agitation, a nano-emulsion system consisting of cationic surfactant (cetyltrimethylammonium bromide, CTAB) and n-hexadecane can be obtained.<sup>31</sup> Due to the presence of cationic surfactant, the nano-emulsions were positive charged, which allowed them to interact with negative charged GO by electrostatic attractions (Fig. S13). The electrostatic interface interaction initiated the assembly synthesis and led to graphene foam with nano-size pores, denoted as PGF-4. SEM images of PGF-4 (Fig. S14 A and B) show highly porous features, with a pore size smaller than 500 nm. TEM analysis identified both wrinkled graphene walls and the frames of near-rectangle pores (Fig. S14 C and D). The pore size is estimated from TEM images (Fig. S14 D) to be  $\sim 200$  nm in width and  $\sim 400$  nm in length. As shown in the nitrogen-sorption analysis result (Fig. S14E), the PGF-4 sample displays a typical type IV curve with a hysteresis loop and a distinct condensation step at a high relative pressure range (0.80 — 0.99). Calculated from the isotherms, PGF-4 has a high surface area of  $451 \text{ m}^2 \text{ g}^{-1}$  and a large total pore volume of  $1.65 \text{ cm}^3 \text{ g}^{-1}$ . Owing to the wrinkled

surface and the hundreds of nanometer pores, the pore size distribution curve exhibits a multi-peak feature (Fig. S14 F).

Micelles can also be adopted as soft-templates to synthesize PGFs. When poly(ethylene oxide)-b-poly(propylene oxide)-b-poly(ethylene oxide) type Pluronic triblock copolymers (e.g. F108) were added into the TMB emulsion system, nano-sized micelles formed.<sup>32</sup> By using such micelles as soft-templates, graphene foams with pores under 100 nm were prepared (PGF-5). Under the SEM observation (Fig. S15 A and B), PGF-5 displays a highly porous structural characteristic. Diameters of the pores are generally smaller than 100 nm. Based on TEM characterization, we found that the pores in PGF-5 were constructed by the packing of graphene nanosheets (Fig. S15 C and D). Nitrogen-sorption results demonstrate that PGF-5 has a high surface area ( $611 \text{ m}^2 \text{ g}^{-1}$ ), large pore volume ( $1.18 \text{ cm}^3 \text{ g}^{-1}$ ) and relatively broad pore size distribution within 100 nm (Fig. S15 E and F). Successful synthesis of PGFs with a pore diameter within  $1 \mu\text{m}$  by nano-emulsions and micelles clearly demonstrates the generality and pore morphology control capability of the as-developed soft-template method.

The PGFs with different structural features have diverse applications. With large open macropores, a highly conductive graphene skeleton ( $35,000 \text{ S m}^{-1}$  for PGF-1) and many edge or defect sites, PGF-1 could serve as an efficient metal-free cathode catalyst for lithium-oxygen batteries.<sup>33-38</sup> The curtailing capacity cycling measurements were conducted to evaluate the electrochemical performance of PGF-1 material. Fig. 3 show the voltage profile and discharge-charge curves of PGF-1 electrode cycled at  $200 \text{ mA g}^{-1}$  with a curtailing capacity of  $1000 \text{ mAh g}^{-1}$ . After 40 cycles, both discharge and charge voltages display excellent stabilities. This is among the best cycling performances of carbonaceous cathodes in  $\text{Li-O}_2$  batteries,<sup>39-40</sup> which is much better than pristine graphene catalysts.<sup>32,36,42,43</sup> Furthermore, the roundtrip electrical efficiency is also high (69.5%, higher than carbon nanotube catalyst (59%)<sup>44</sup>) and stable (92.1% retention) (Fig. S16). Therefore, PGF-1 could have potential as catalysts for  $\text{Li-O}_2$  batteries with high performances.

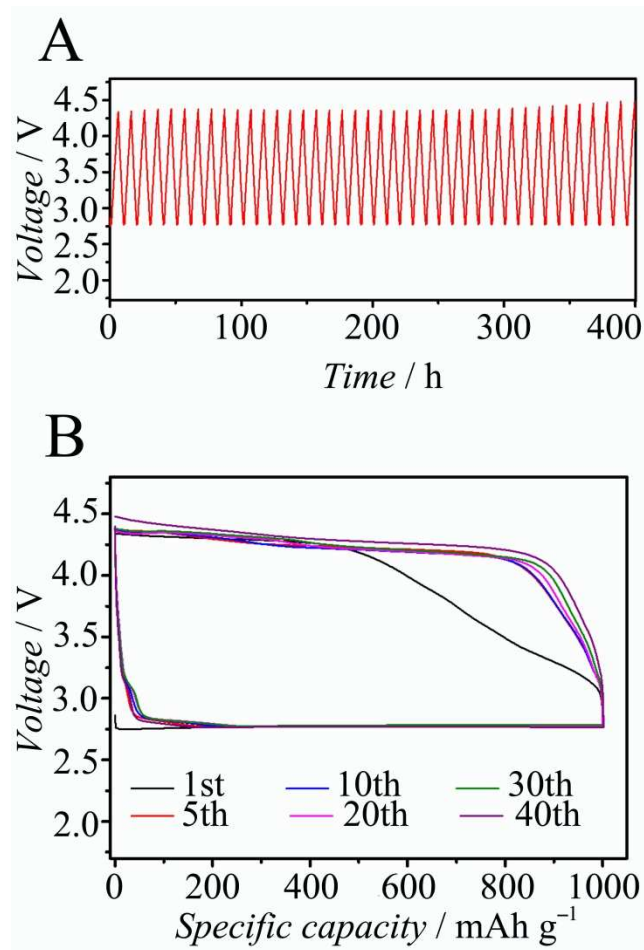


**Figure 3.** Electrochemical performances of PFG-1 as cathode catalyst in Li-O<sub>2</sub> batteries. Cell voltage profiles upon completion of each charge-discharge (A) and Charge-discharge profiles of the cell at various cycle numbers (B) at 200 mA g<sup>-1</sup> with a curtailing capacity of 1000 mAh g<sup>-1</sup>.

For comparison, none porous graphene (Fig. S6 sample) and PGF-5 were also tested as cathodes. However, both of these two materials show much poor cycling performances than PGF-1 (Fig. S 17 and 18). The charge-discharge potential gaps continuously increase within only 20 cycles, indicating strong electrode polarizations. Comparing to the structure features, PGF-1 sample with micron-size macroporous texture appears to be the most suitable material as catalysts for Li-O<sub>2</sub> batteries. To investigate the mechanism, surface morphologies of PGF-1 electrode at different states were monitored by *ex-situ* SEM (Fig. 4). When fully discharging the cell in the first cycle, large amounts of toroid Li<sub>2</sub>O<sub>2</sub> nanocrystals (confirmed by X-ray diffraction, Fig. S19) were formed on the surface of PGF-1 (Fig. 4B). The size of Li<sub>2</sub>O<sub>2</sub> nanocrystals are around 300 nm, which requires large pores to accommodate. Although PGF-5 has high surface area under nitrogen-sorption analysis, the small pores restrain the efficient utilization of porous surface. Thus, the performance of PGF-5 is just similar to none porous graphene and much worse than PGF-1. After subsequent charges, most discharge products disappeared (Fig. 4c), indicating a high catalytic activity of PGF-1 material as cathode in Li-O<sub>2</sub> batteries.

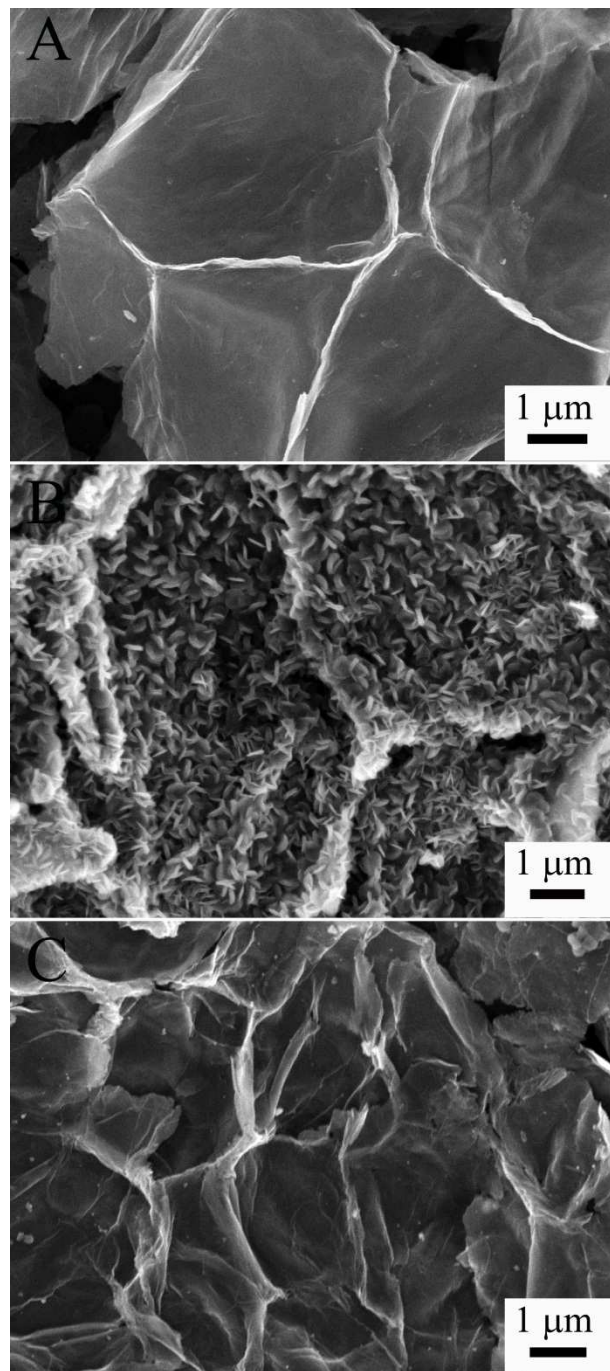


**Figure 4.** Morphology changes of the PGF-1 electrode at different states during discharge/charge cycle. (A) SEM image of the electrode before cycling. (B) SEM image of electrode at the fully discharge state in the first cycle. (C) SEM image of the electrode at the fully charged state in the first cycle.

PGFs can also be found in applications for high-efficiency adsorption, which is crucial for the separation/extraction of oils or other organic pollutants. PGF-2 with a hierarchical macroporous structure exhibits an impressive performance for the adsorption of model oil molecules. The graphene walls offer  $\pi$ -conjugation and the hydrophobic surface to attract oil molecules from water. Furthermore, the large exposed surfaces enable PGF-2 to adsorb oils from aqueous solutions and store in

the pore voids.<sup>19</sup> As shown in Fig. 4, 250  $\mu\text{l}$  dyed toluene, hexadecane and olive oil can be completely adsorbed by 6 mg PGF-2 within 2 minutes ( $41.7 \mu\text{l mg}^{-1}$ ). Although carbon nanotube modified CVD graphene foams<sup>16</sup> showed higher oil adsorbing capacities, the PGF-2 sample still demonstrated a better performance than pure graphene capsules ( $17.5$  to  $21.0 \mu\text{l mg}^{-1}$ )<sup>19</sup> for oil adsorption. Moreover, PGF-2 can be recycled by direct combustion in air, showing remarkable thermal stability and recyclable usage (Fig. 6, movie S-1).

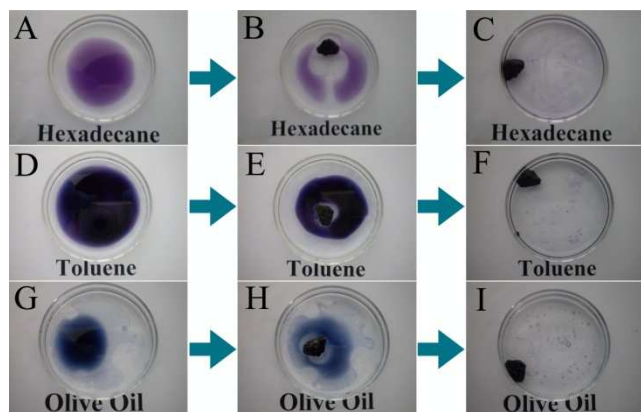


**Figure 5.** Oil adsorption demonstrations of the sample PGF-2. (A), (D) and (G) are digital photos of 250  $\mu\text{l}$  of different oils in H<sub>2</sub>O; (B), (E) and (H) after adding 6 mg of PGF-2, oils were absorbed subsequently. (C), (F) and (I) reaching complete adsorption, the majority of hexadecane was removed.

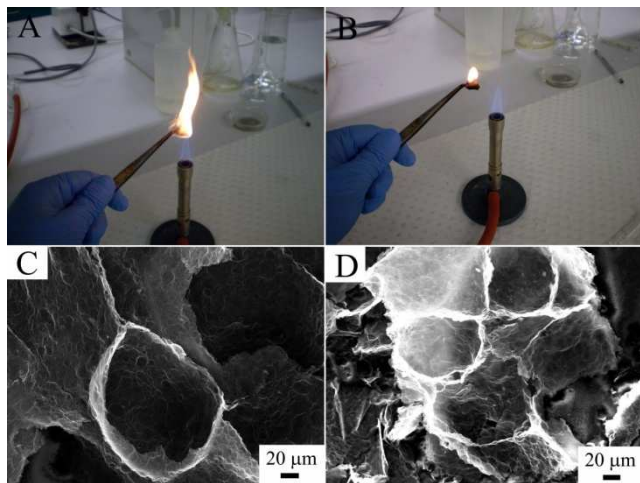


**Figure 6.** Combustion recycling of PGF-2 (hexadecane adsorption). (A), (B) Digital photos of combustion. Independent combustion (B) confirmed that PGF-2 contained large amount of hexadecane inside. (C) and (D) SEM images of PGF-2, before and after burning in air, respectively. After complete combustion, hierarchical porous architecture maintained very well, suggesting a good thermal stability of PGF-2.

## Conclusions

In summary, we have developed a general emulsion soft-template approach to synthesize porous graphene foams with controlled pore morphologies. Multiple emulsions and micelles were employed to synthesize porous graphene foams with

diverse structural features. Specific interfacial interactions and suitable reaction conditions have been proved to be essential for the regular graphene oxide/template assembly and the preparation of graphene foams. We also demonstrated that porous graphene foams had promising applications for Li-O<sub>2</sub> batteries and oil adsorptions. Due to the novel porous structures, PGFs exhibited an excellent stability as cathode catalysts in Li-O<sub>2</sub> batteries and delivered high efficiency for oil adsorptions.

## Acknowledgements

This work was financially supported by the Australian Research Council (ARC) through the ARC FT project (FT110100800) and ARC Discovery project (DP1093855).

## Notes and references

<sup>a</sup> Centre for Clean Energy Technology, School of Chemistry and Forensic Science, University of Technology Sydney, NSW 2007, Australia. E-mail: Guoxiu.Wang@uts.edu.au (GXW)

<sup>b</sup> Department of Chemistry and Shanghai Key Laboratory of Molecular Catalysis and Innovative Materials, Fudan University, Shanghai 200433, P. R. China. E-mail: dyzhao@fudan.edu.cn (DYZ)

† Footnotes should appear here. These might include comments relevant to but not central to the matter under discussion, limited experimental and spectral data, and crystallographic data.

Electronic Supplementary Information (ESI) available: experimental details and characterizations of PGFs and their intermediates; characterizations of lithium-oxygen battery electrodes; digital photos and movies of oil adsorptions. See DOI: 10.1039/b000000x/

- 1 A. H. Lu, G.-P. Hao, Q. Sun, *Angew. Chem. Int. Ed.*, 2013, **52**, 7930.
- 2 Z. S. Wu, S. Yang, Y. Sun, K. Parvez, X. Feng, K. Muellen, *J. Am. Chem. Soc.*, 2012, **134**, 9082.
- 3 Z. S. Wu, A. Winter, L. Chen, Y. Sun, A. Turchanin, X. Feng, K. Muellen, *Adv. Mater.*, 2012, **24**, 5130.
- 4 H. Sun, Z. Xu, C. Gao, *Adv. Mater.*, 2013, **25**, 2554.
- 5 Z. Y. Wu, C. Li, H.-W. Liang, J.-F. Chen, S.-H. Yu, *Angew. Chem. Int. Ed.*, 2013, **52**, 2925.
- 6 Y. Zhao, C. Hu, Y. Hu, H. Cheng, G. Shi, L. Qu, *Angew. Chem. Int. Ed.*, 2012, **51**, 11371.
- 7 S. H. Lee, H. W. Kim, J. O. Hwang, W. J. Lee, J. Kwon, C. W. Bielawski, R. S. Ruoff, S. O. Kim, *Angew. Chem. Int. Ed.*, 2010, **49**, 10084.
- 8 L. Qiu, J. Z. Liu, S. L. Y. Chang, Y. Wu, D. Li, *Nat. Commun.*, 2012, **3**, DOI: 10.1038/ncomms2251.
- 9 Z. Chen, W. Ren, L. Gao, B. Liu, S. Pei, H.-M. Cheng, *Nat. Mater.*, 2011, **10**, 424.
- 10 Y. Wan, D. Zhao, *Chem. Rev.*, 2007, **107**, 2821.
- 11 Y. Deng, J. Wei, Z. Sun, D. Zhao, *Chem. Soc. Rev.*, 2013, **42**, 4054.
- 12 Y. Shi, Y. Wan, D. Zhao, *Chem. Soc. Rev.*, 2011, **40**, 3854.
- 13 Y. Zhai, Y. Dou, D. Zhao, P. F. Fulvio, R. T. Mayes, S. Dai, *Adv. Mater.*, 2011, **23**, 4828.
- 14 X. Cao, Y. Shi, W. Shi, G. Lu, X. Huang, Q. Yan, Q. Zhang, H. Zhang, *Small*, 2011, **7**, 3163.
- 15 X. C. Dong, H. Xu, X. W. Wang, Y. X. Huang, M. B. Chan-Park, H. Zhang, L. H. Wang, W. Huang, P. Chen, *ACS Nano*, 2012, **6**, 3206.

- 16 X. C. Dong, J. Chen, Y. W. Ma, J. Wang, M. B. Chan-Park, X. M. Liu, L. H. Wang, W. Huang, P. Chen, *Chem. Commun.*, 2012, **48**, 10660.
- 17 X. Huang, K. Qian, J. Yang, J. Zhang, L. Li, C. Yu and D. Zhao, *Adv. Mater.*, 2012, **24**, 4419.
- 18 D. Fan, Y. Liu, J. He, Y. Zhou and Y. Yang, *J. Mater. Chem.*, 2012, **22**, 1396.
- 19 K. Sohn, Y. J. Na, H. Chang, K.-M. Roh, H. D. Jang, J. Huang, *Chem. Commun.*, 2012, **48**, 5968.
- 20 B. G. Choi, M. Yang, W. H. Hong, J. W. Choi, Y. S. Huh, *ACS Nano*, 2012, **6**, 4020.
- 21 Y. Meng, D. Gu, F. Zhang, Y. Shi, L. Cheng, D. Feng, Z. Wu, Z. Chen, Y. Wan, A. Stein, D. Zhao, *Chem. Mater.*, 2006, **18**, 4447.
- 22 Y. Meng, D. Gu, F. Q. Zhang, Y. F. Shi, H. F. Yang, Z. Li, C. Z. Yu, B. Tu, D. Y. Zhao, *Angew. Chem. Int. Ed.*, 2005, **44**, 7053.
- 23 S. Yin, Y. Zhang, J. Kong, C. Zou, C. M. Li, X. Lu, J. Ma, F. Y. C. Boey, X. Chen, *ACS Nano*, 2011, **5**, 3831.
- 24 J. Kim, L. J. Cote, F. Kim, W. Yuan, K. R. Shull, J. Huang, *J. Am. Chem. Soc.*, 2010, **132**, 8180.
- 25 L. Qiu, X. Yang, X. Gou, W. Yang, Z.-F. Ma, G. G. Wallace, D. Li, *Chem. Eur. J.*, 2010, **16**, 10653.
- 26 K. P. Loh, Q. Bao, G. Eda, M. Chhowalla, *Nat. Chem.*, 2010, **2**, 1015.
- 27 M. Zhang, L. Bai, W. Shang, W. Xie, H. Ma, Y. Fu, D. Fang, H. Sun, L. Fan, M. Han, C. Liu, S. Yang, *J. Mater. Chem.*, 2012, **22**, 7461.
- 28 S. Park, R. S. Ruoff, *Nat. Nanotech.*, 2009, **4**, 217.
- 29 D. Li, M. B. Mueller, S. Gilje, R. B. Kaner, G. G. Wallace, *Nat. Nanotech.*, 2008, **3**, 101.
- 30 D. Suzuki, S. Tsuji, and H. Kawaguchi, *J. Am. Chem. Soc.*, 2007, **129**, 8088.
- 31 S. H. Wu, Y. Hung, C. Y. Mou, *Chem. Mater.*, 2013, **25**, 352.
- 32 J. W. Tang, X. F. Zhou, D. Y. Zhao, G. Q. Lu, J. Zou, C. Z. Yu, *J. Am. Chem. Soc.*, 2007, **129**, 9044.
- 33 Y. Li, J. Wang, X. Li, D. Geng, R. Li, X. Sun, *Chem. Commun.*, 2011, **47**, 9438.
- 34 J. Xiao, D. Mei, X. Li, W. Xu, D. Wang, G. L. Graff, W. D. Bennett, Z. Nie, L. V. Saraf, I. A. Aksay, J. Liu, J.-G. Zhang, *Nano Lett.*, 2011, **11**, 5071.
- 35 E. Yoo, H. Zhou, *ACS Nano*, 2011, **5**, 3020.
- 36 B. Sun, B. Wang, D. Su, L. Xiao, H. Ahn, G. Wang, *Carbon*, 2012, **50**, 727.
- 37 B. Sun, P. Munroe and G. Wang, *Sci. Rep.*, 2013, **3**, 2247.
- 38 J. J. Wang, Y. L. Li, X. L. Sun, *Nano Energy*, 2013, **2**, 443.
- 39 G. Wu, N. H. Mack, W. Gao, S. Ma, R. Zhong, J. Han, J. K. Baldwin, P. Zelenay, *ACS Nano*, 2012, **6**, 9764.
- 40 H. Wang, Y. Yang, Y. Liang, G. Zheng, Y. Li, Y. Cui, H. Dai, *Energy Environ. Sci.*, 2012, **5**, 7931.
- 41 Z. Guo, D. Zhou, X. Gong, Z. Qiu, Y. Wang, Y. Yao, *Adv. Mater.*, 2013, **25**, 5668.
- 42 Y. Li, J. Wang, X. Li, D. Geng, M. N. Banis, R. Li, X. Sun, *Electrochem. Commun.*, 2012, **18**, 12.
- 43 D. Xu, Z. L. Wang, J. J. Xu, L. L. Zhang, X. B. Zhang, *Chem. Commun.*, 2012, **48**, 6948.
- 44 Z. L. Jian, P. Liu, F. J. Li, P. He, X. W. Guo, M. W. Chen, H. S. Zhou, *Angew. Chem. Int. Ed.*, 2014, **53**, 442.